Journal of Fluorescence
https://doi.org/10.1007/s10895-024-03856-w

RESEARCH

A New Phenothiazine-Based Fluorescent Probe for Rapid and Specific Detection of Fluoride

Ying Zhang[1] · Tingting Feng[1] · Taozhu Hu[1] · Yi Wang[1] · Yi Le[1,2]

Received: 23 May 2024 / Accepted: 15 July 2024

Abstract
Fluorescent probes with specific and rapid response to fluoride ions are important mediators for detecting fluoride ions in biological systems. In this study, a phenothiazine-based fluorescent probe, **PTC**, was designed and synthesized, which undergoes cleavage activation and cyclization induced by fluoride ions targeting Si–O bonds. The probe exhibits strong anti-interference properties and reaches peak fluorescence within 5 min, allowing for quantitative detection of fluoride ions content in the concentration range of 0 to 12.5μM, suitable for live cell fluorescence imaging. The research findings suggest its potential application value in biological systems.

Keywords Phenothiazine · Fluoride · Fluorescence · Probe · Cell imaging

Introduction

Fluoride ions, the smallest and most electronegative anions, are of paramount importance to organisms [1–4]. Adequate intake of F^- plays a crucial role in health, such as maintaining skeletal structure and physiological functions [5–8]. However, excessive fluoride can have harmful effects on health, including acute and chronic fluoride poisoning, fluorosis, neurodegenerative diseases, gastric and renal issues, and even death [9–16]. Therefore, developing highly selective and sensitive detection and quantification methods for fluoride ions to visualize their distribution in organisms is crucial [17–24].

Fluorescence sensing is considered an ideal technique among commonly used methods like colorimetry [25, 26], atomic absorption spectroscopy, and ion chromatography for F^- detection [27, 28], especially in bioimaging applications due to its non-invasive and real-time nature [29–33]. Currently, despite significant progress in the development of F^- fluorescent probes, there are still some drawbacks in their application in live cells and in vivo, such as high background interference, insufficient sample penetration, and long response times. Therefore, designing fluoride ion probes that can rapidly respond and have a large Stokes shift remains a challenge that needs to be addressed [34–37].

Therefore, we have designed a new fluorescence probe, **PTC**, for detecting fluoride ions in cells. It utilizes a fluorescein moiety and relies on fluoride-induced Si–O bond cleavage as its recognition mechanism (Scheme 1). We aim to develop a fluorescence probe with fast response time, large Stokes shift, and excellent specificity for fluorescence imaging of fluoride ions in live cells.

Experimental

Materials and Instruments

All chemicals were sourced as analytical-grade from Energy Chemical Ltd. (Shanghai) and Sigma-Aldrich (Shanghai) Co., Ltd. NMR spectra (^1H and ^{13}C) were recorded on a Bruker (Avance) 400 MHz NMR instrument at Guizhou University's School of Pharmacy. Absorption spectra were captured on a UV-5500PC UV–Vis spectrophotometer, and fluorescence spectra were measured using a Hitachi F4700 fluorescence spectrometer, both provided by Guizhou University's School of Pharmacy. Mass spectra were obtained using a TSQ 8000 high-resolution mass spectrometer (Thermo Fisher Scientific Co., Ltd.). Melting

✉ Yi Le
yile2021@163.com

[1] School of Pharmaceutical Sciences, Guizhou University, Guiyang 550025, China

[2] Guizhou Engineering Laboratory for Synthetic Drugs, Guiyang 550025, China

Published online: 22 July 2024

Scheme 1 Recognition mechanism of **PTC** for F^-

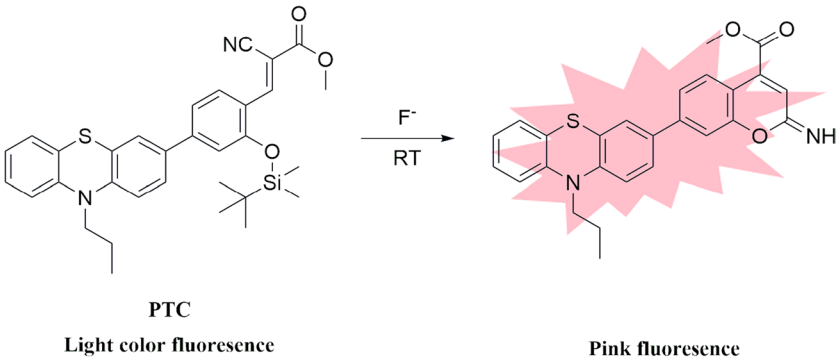

points were determined with an X-4X digital melting point apparatus (uncorrected, Shanghai Microelectronics Technology Co., Ltd.). For biological imaging, an inverted fluorescence microscope (NIB600, Ningbo Novel Co., Ltd.) was utilized.

Preparation and Measurement of Probe Solutions

To prepare a 1 mM **PTC** stock solution, the probe **PTC** was dissolved in DMSO. A stock solution of tetrabutylammonium fluoride (TBAF) at a concentration of 100 mM was produced using THF. Analytes were made as 100 mM stock solutions in deionized water for storage, including common cations (Na^+, Ca^{2+}, K^+, Fe^{2+}, Fe^{3+}, Cu^{2+}, Ag^+, Zn^{2+}) and anions (Cl^-, Br^-, I^-, SO4 $^{2-}$, HSO_3^-, $H_2PO_4^{2-}$, HCO_3^-, SCN^-, NO_3^-, HPO_4^-). The fluorescence spectra of **PTC** for various analytes were investigated using 4 mL of DMSO solution at room temperature. Unless otherwise noted, fluorescence spectra were typically collected after 1 h of analyte addition. All aqueous solutions were made using ultrapure water from a Milli-Q purifier.

Cell Cytotoxicity Assay and Cell Image

Human hepatocellular carcinoma cells (HepG2 cells) were procured from the Kunming Cell Bank of Chinese Academy of Sciences and maintained in our laboratory. The cytotoxicity of the probe **PTC** against HepG2 cells was evaluated using the MTT assay. HepG2 cells were sown in 96-well plates and cultivated for 24 h. **PTC** solutions at different concentrations (0, 1, 5, 10, and 20 μM) were added, incubated with cells for 24 h. The MTT assay was performed using the literature methods [38]. In cellular imaging experiments, HepG2 cells were initially incubated with **PTC** (3 μM, in PBS) for 30 min, then TBAF (200 μM) was added, further incubated for 30 min. After three times washes with PBS, imaging was performed using laser confocal scanning microscopy.

Synthesis and Characterization

Synthesis of Compound 2

Thiophene boronic acid ester (367 mg, 1 mmol) was added to a round-bottom flask containing Dioxane/H_2O (1:1, 5 mL), followed by the addition of 4-bromo-2-methoxybenzaldehyde (215 mg, 1.1 mmol) and anhydrous Na_2CO_4 (212 mg, 2 mmol). Subsequently, $Pd(PPh_3)_4$ (11.55 mg, 0.01 mmol) was introduced under argon protection, and the reaction was carried out at 110 ℃ for 3 h. After cooling to room temperature, the reaction was quenched with water (5 mL), and the mixture was extracted with DCM (10 mL × 3). The combined organic phases were washed with saturated brine, dried over anhydrous Na_2SO_4, and concentrated under vacuum. The resulting crude product was purified by column chromatography (eluent: PE:EA = 5:1; stationary phase: 200–300 mesh silica gel) to afford compound **2** as pale yellow oil (220 mg, 58.7% yield). ^{1}H NMR (400 MHz, $CDCl_3$) δ 10.45 (d, J = 0.8 Hz, 1H), 7.85 (d, J = 8.0 Hz, 1H), 7.43 – 7.35 (m, 2H), 7.19 – 7.13 (m, 3H), 7.08 (d, J = 1.6 Hz, 1H), 6.95 – 6.86 (m, 3H), 3.98 (s, 3H), 3.87 – 3.83 (m, 2H), 1.89 – 1.83 (m, 2H), 1.03 (t, J = 7.6 Hz, 3H). ^{13}C NMR (100 MHz, $CDCl_3$) δ 189.4, 162.2, 147.8, 145.8, 144.7, 134.0, 129.1, 127.5, 127.4, 126.2, 125.9, 125.5, 124.1, 123.4, 122.7, 118.9, 115.6, 109.4, 55.7, 49.3, 20.1, 11.3. ESI-HRMS $C_{23}H_{21}NO_2S$ ($[M+H]^+$): calcd 376.1366, found 376.1360.

Synthesis of Compound 3

$AlCl_3$ (1.16 g, 9 mmol) was introduced into a pear-shaped flask, followed by the addition of anhydrous CH_2Cl_2 (10 ml). Compound **2** (1.08 g, 3 mmol) was dissolved in anhydrous CH_2Cl_2 (5 mL) and carefully added dropwise. The reaction proceeded at ambient temperature for 12 h. Upon completion, HCl solution (2 mol/L, 8 mL) was added dropwise and stirring continued for an additional 0.5 h.

Following stirring, the organic solvent was evaporated under reduced pressure. The residual liquid was subsequently subjected to extraction with EA (20 mL × 3), and the combined organic phases were then washed with saturated brine, dried over anhydrous Na_2SO_4, and concentrated under vacuum. The resulting crude product underwent purification via column chromatography (eluent: PE:EA = 5:1; stationary phase: 200–300 mesh silica gel) to afford compound **3** as yellow-green solid (0.85 g, 81.2% yield). M.P: 98.3–99.4℃.^{1}H NMR (400 MHz, DMSO) δ 11.06 – 10.60 (m, 1H), 10.22 (d, *J* = 1.6 Hz, 1H), 7.71 (dd, *J* = 8.0, 1.6 Hz, 1H), 7.53 (dt, *J* = 8.4, 2.0 Hz, 1H), 7.47 (d, *J* = 2.0 Hz, 1H), 7.26 (d, *J* = 8.0 Hz, 1H), 7.24 – 7.19 (m, 2H), 7.17 (d, *J* = 7.6 Hz, 1H), 7.10 (dd, *J* = 8.4, 1.6 Hz, 1H), 7.04 (d, *J* = 8.0 Hz, 1H), 6.96 (t, *J* = 7.6 Hz, 1H), 3.88 (d, *J* = 14.0 Hz, 2H), 1.73 (p, *J* = 7.2 Hz, 2H), 0.96 (td, *J* = 7.6, 1.6 Hz, 3H).^{13}C NMR (100 MHz, $CDCl_3$) δ 195.8, 162.0, 148.6, 146.1, 144.6, 134.1, 133.2, 127.5, 127.4, 126.3, 126.0, 125.5, 124.1, 122.8, 119.3, 118.1, 115.6, 115.5, 114.8, 49.3, 20.1, 11.3. ESI-HRMS $C_{22}H_{19}NO_2S$ ($[M+H]^+$): calcd 362.120926, found 362.11946.

Synthesis of Compound 4

Compound **3** (100 mg, 1 mmol) was added to a two-neck flask along with DCM (5 mL), followed by the addition of DMAP (44 mg, 0.36 mmol) and TEA (91 mg, 0.9 mmol) under argon protection, and cooled to 0 ℃. Finally, tert-butyldimethylchlorosilane (181 mg, 1.2 mmol) was dissolved in DCM (5 mL) and added dropwise. The reaction mixture was stirred at room temperature for 12 h. Upon completion, deionized water (10 mL) was added to quench the reaction, and the mixture was extracted with DCM (10 mL × 3). The combined organic phases were washed with saturated brine, dried over anhydrous Na_2SO_4, and concentrated under vacuum. The resulting crude product was purified by column chromatography (eluent: PE:EA = 5:1; stationary phase: 200–300 mesh silica gel) to yield compound **4** as yellow-green oil (120 mg, 84% yield). ^{1}H NMR (400 MHz, $CDCl_3$) δ 10.44 (d, *J* = 0.8 Hz, 1H), 7.84 (d, *J* = 8.0 Hz, 1H), 7.37 – 7.32 (m, 2H), 7.21 – 7.13 (m, 3H), 7.00 (d, *J* = 1.6 Hz, 1H), 6.95 – 6.87 (m, 3H), 3.87 – 3.83 (m, 2H), 1.89 – 1.83 (m, 2H), 1.04 (d, *J* = 5.6 Hz, 12H), 0.31 (s, 6H). ^{13}C NMR (100 MHz, $CDCl_3$) δ 189.6, 159.2, 147.5, 145.7, 133.8, 128.8, 127.5, 127.4, 126.1, 125.7, 124.2, 122.8, 119.8, 117.8, 115.6, 115.6, 49.3, 27.0, 25.7, 18.4, 11.3. ESI-HRMS $C_{28}H_{33}NO_2SSi$ ($[M+Na]^+$): calcd 498.189348, found 498.18874.

Synthesis of Compound PTC

Compound **4** (950.4 mg, 2 mmol) was added to a round-bottom flask containing anhydrous THF (15 mL), followed by the addition of methyl cyanoformate (99 mg, 4 mmol), and tetrahydrofuran (0.53 mg, 0.0075 mmol), under argon protection, and the reaction mixture was cooled to 0 ℃ and stired for 4 h. Upon completion, the solvent was removed under vacuum, and the crude product was purified by column chromatography (eluent: PE:EA = 5:1; stationary phase: 200–300 mesh silica gel) to yield compound **PTC** as orange solid (420 mg, 37.7% yield). M.P:120.1–121.2℃. IR (KBr, ν, cm^{-1}): 2948.7, 1709.6, 1579.1, 1467.0, 1245.2, 1135.65, 966.1. ^{1}H NMR (400 MHz, DMSO) δ 8.69 (d, *J* = 3.6 Hz, 1H), 8.29 (dd, *J* = 22.4, 8.4 Hz, 1H), 7.56 (d, *J* = 8.0 Hz, 2H), 7.23 (dd, *J* = 13.6, 8.6 Hz, 3H), 7.16 (d, *J* = 8.6 Hz, 1H), 7.09 (d, *J* = 8.0 Hz, 1H), 7.01 (t, *J* = 7.6 Hz, 1H), 3.91 (d, *J* = 10.4Hz, 5H), 1.77 (q, *J* = 7.2 Hz, 2H), 1.07 – 0.88 (m, 12H), 0.34 (s, 5H). ^{13}C NMR (100 MHz, $CDCl_3$) δ 163.6, 157.2, 149.6, 146.8, 145.8, 144.6, 133.4, 129.6, 127.5, 127.4, 126.1, 125.7, 125.6, 124.1, 122.8, 121.7, 120.1, 117.1, 116.2, 115.7, 115.6, 100.0, 53.1, 49.4, 25.7, 20.1, 18.3, 11.3. ESI-HRMS $C_{32}H_{36}N_2O_3SSi$ ($[M+Na]^+$): calcd 579.210811, found 597.20996.

Results and Discussion

Synthesis

The fluorescent probe **PTC**, with a benzothiazole moiety as the fluorophore and utilizing Si–O bonds as recognition groups, was synthesized. Starting from benzothiazole boronate, it underwent a series of reactions including Suzuki coupling (yield: 58.7%), demethylation (yield: 81.2%), nucleophilic substitution (yield: 84%), and nucleophilic addition (yield: 37.7%), as depicted in Scheme 2, resulting in an overall yield of 15.1%. The structural characterization data for all intermediates and the probe can be found in the supporting information (Figures S1-S13). Mass spectrometric analysis of the fluorescent substance generated by the reaction of probe **PTC** with fluoride ions (Figure S14) showed consistency with the predicted reaction product, validating the fluorescence detection mechanism of this probe.

Photophysical Properties

Absorption and Fluorescence Spectrum of PTC

The detection capability of the probe **PTC** for fluoride ions was investigated using absorption spectroscopy and fluorescence spectroscopy. As shown in Fig. 1a, the first absorption band of **PTC** (30 μM DMSO) appears at 425 nm. Upon response to fluoride ions in DMSO solution, the absorption band shifts to around 520 nm, with an isosbestic point emerging at 475 nm. Figure 1b illustrates that under an excitation wavelength of 520 nm, the probe

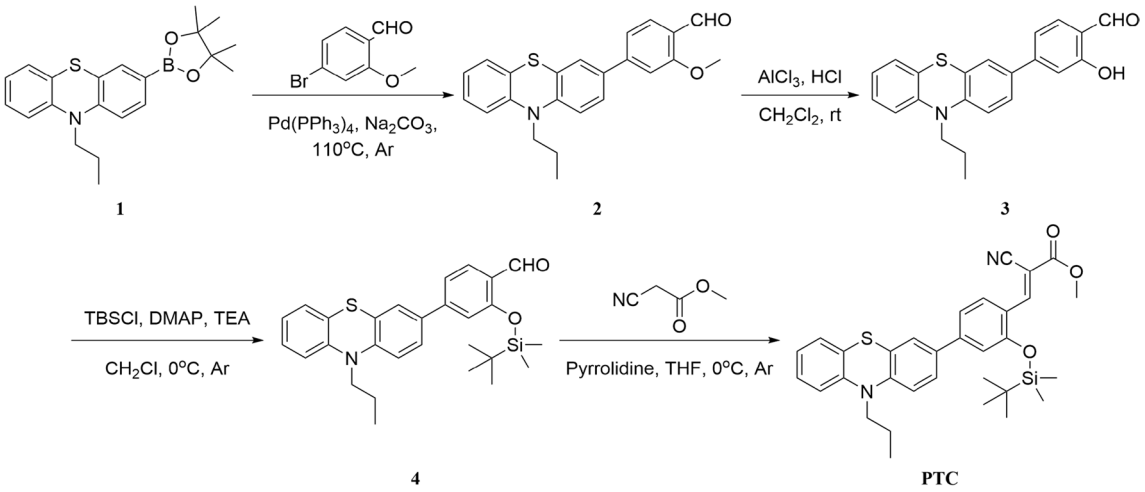

Scheme 2 Synthetic route of **PTC**

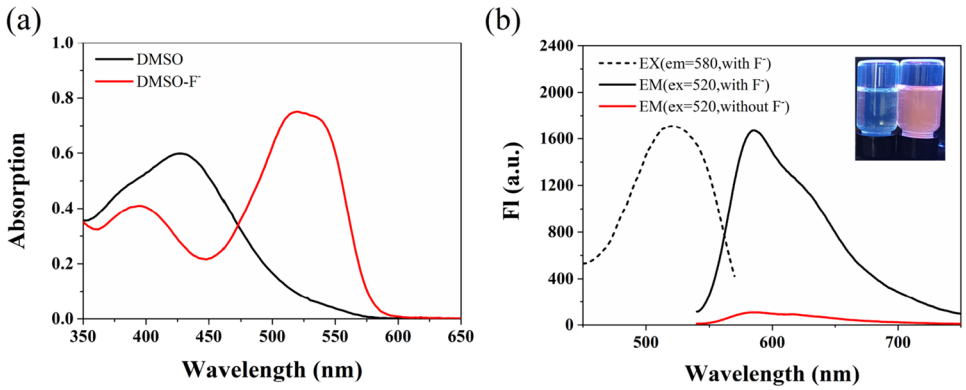

Fig. 1 (**a**) Absorption spectra of probe **PTC** (30 μM) in DMSO solvent with (3 mM) and without F^- at room temperature; (**b**) Fluorescence spectra of probe **PTC** (5 μM) in DMSO solution with and without F^- (0.5 mM) at room temperature; Insert: color change of solution with and without F^- under 365 nm light

PTC exhibits weak fluorescence at 580 nm. Upon addition of F^-, the fluorescence intensity at 580 nm significantly increases under the same excitation wavelength, with the solution color turning pink. Furthermore, spectra of the probe **PTC** response to F^- were recorded separately at an excitation wavelength of 580 nm and 520 nm, forming a mirror relationship with the emission spectrum. The result shows that, in DMSO solution, the response of the probe **PTC** to fluoride ions is evident, accompanied by a change in solution color from light to pink, had the ability to detect F^-.

The excitation and emission peaks intersect, termed the fluorescence resonance energy transfer (FRET) mechanism. Four common strategies construct fluorescence probes using FRET [39]. This study transforms non-fluorescent receptors into fluorescent structures. In the **PTC** molecule, the phenothiazine ring serves as the fluorescent donor, with the receptor as a substituent on this ring. Fluorescence at 580nm is minimal without F^-. Upon reacting with F^-, a new ring forms, initiating FRET and yielding strong emission fluorescence at 580 nm.

Fluorescence Spectra of in Different Solvents

Subsequently, the fluorescence response of probe **PTC** to F^- in various solvents was investigated (Fig. 2). The results reveal that its fluorescence response is most pronounced in THF solution. In acetone (DMK), acetonitrile (CAN), and DMSO solvents, probe **PTC** also demonstrates a noticeable fluorescence response to F^-, with significant changes in fluorescence intensity observed pre- and post-fluoride ion addition. Considering the favorable biocompatibility of DMSO, it was selected as the foundational solvent for subsequent performance tests.

Response Time of PTC

Building on the favorable fluorescence characteristics of probe **PTC** in DMSO solution, we conducted a detailed examination of the fluorescence intensity variations of probe **PTC** in response to F^- at various time intervals in DMSO solution to elucidate its response kinetics to F**-**. As illustrated in Fig. 3, the fluorescence intensity of the solution peaked

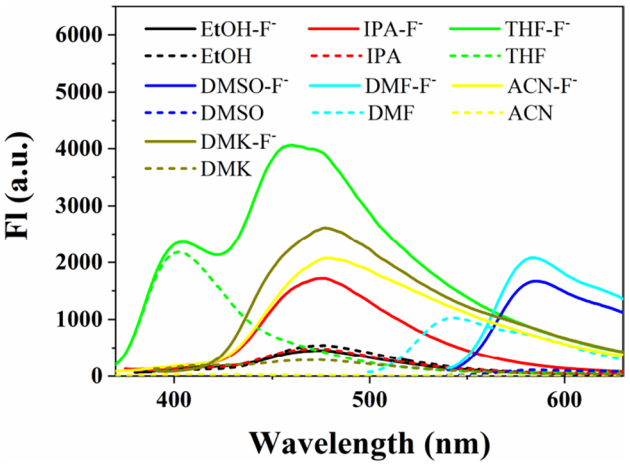

Fig. 2 Fluorescence spectra of **PTC** (5 μM) in various solvents with and without F^- (0.5 mM)

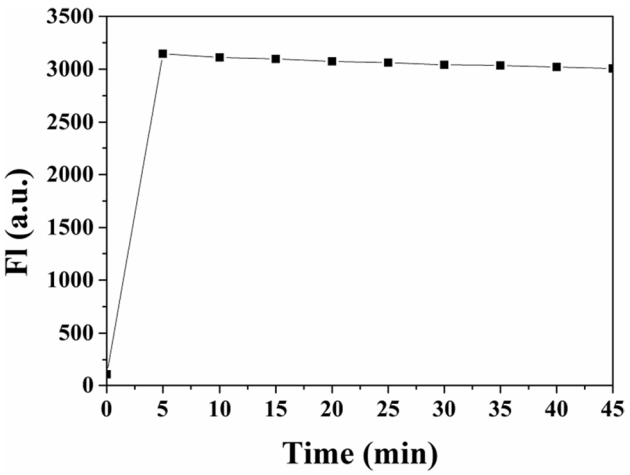

Fig. 3 Time-dependent fluorescence intensity of **PTC** (5 μM) to F^- (0.5 mM), λ_{ex} = 520 nm, λ_{em} = 580 nm

at 3200 a.u. within 5 min post addition of fluoride ions and remained relatively constant within 45 min. This observation suggests that **PTC** exhibits a rapid and substantial response to fluoride ions, manifested by notable changes in fluorescence intensity.

Job's Curve and Detection Limit of PTC

To investigate the quantitative relationship between probe **PTC** and F^- concentrations, fluorescence titration spectroscopy was employed. Figure 4a illustrates that at an excitation wavelength of 520 nm, the solution exhibited its maximum emission fluorescence at 580 nm. As the equivalent ratio of F^- to probe **PTC** increased, the fluorescence intensity of the solution gradually intensified. Within the range of 0 to 12.5 μM, the fluorescence intensity exhibited a linear correlation with F^- concentration (y = 124.49143C + 1084.7619, R^2 = 0.98773) (Fig. 4b). The detection limit (LOD) was calculated using the formula LOD = 3 σ/κ and was found to be 0.51 μM.

Selectivity of PTC

To ensure the precise recognition of the target by probe **PTC**, a comprehensive array of common cations (Na^+, Ca^{2+}, K^+, Fe^{2+}, Fe^{3+}, Cu^{2+}, Ag^+, Zn^{2+}) and anions (Cl^-, Br^-, I^-, SO_4^{2-}, HSO_3^-, $H_2PO_4^{2-}$, HCO_3^-, SCN^-, NO_3^-, HPO_4^-) were utilized as interferents to assess the selectivity of probe **PTC** towards F^-. The outcomes, as illustrated in Fig. 5, reveal minimal interference from common cations and anions, thereby affirming the probe's efficacy in detecting F^- within complex biological environments.

Cell Imaging of PTC

Initially, the cytotoxicity of probe **PTC** towards HepG2 cells was assessed using the MTT colorimetric method. HepG2 cells were treated with probe **PTC** at concentrations ranging from 0 to 20 μM. The results (Fig. 6) indicate minimal toxicity of **PTC**, with the cell viability remaining at 90%

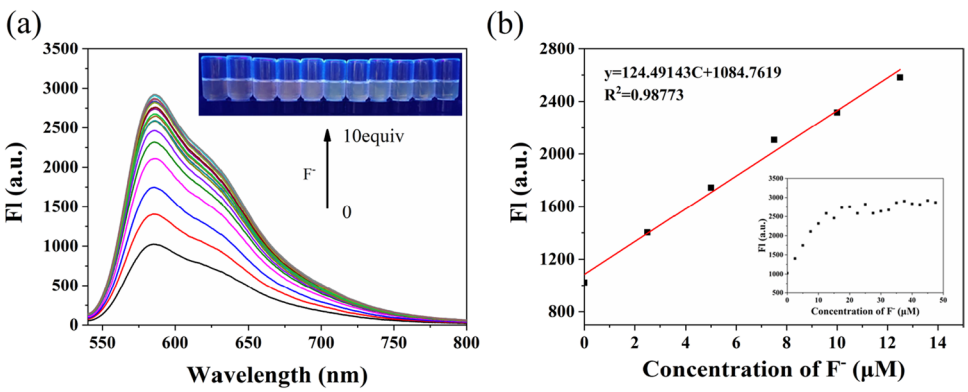

Fig. 4 (**a**) Fluorescence titration of **PTC** (5 μM) upon of F^- (0–47.5 μM); Insert: the fluorescence changes with F^- concentration (0–47.5 μM) under 365 nm light; (**b**) Linear correlation between the intensity of fluorescence and F^- concentration (0–12.5 μM), λ_{ex} = 520 nm, λ_{em} = 580 nm; Inset: the correlation between the fluorescence intensity and F^- concentration (0–47.5 μM), λ_{ex} = 520 nm

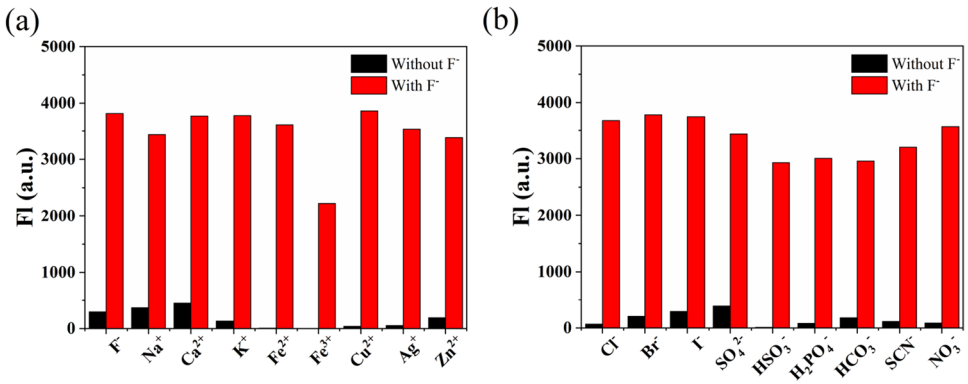

Fig. 5 Fluorescence intensity of **PTC** (5 μM) with and without F^- (0.5 mM) in the presence of other cations and anions. (**a**) various cations (sodium salt, 0.5 mM); (**b**) various anions (sulfate, 0.5 mM). $\lambda_{ex} = 520$ nm, $\lambda_{em} = 580$ nm

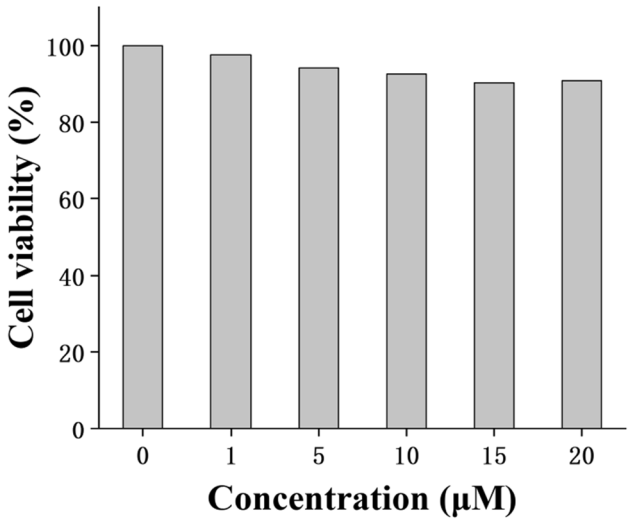

Fig. 6 Cell viability of HepG2 cells treated with **PTC** (0–20 μM) after 24 h

even at a compound concentration of 20 μM. Subsequently, selecting a concentration of 5 μM for probe **PTC** in cellular imaging experiments is feasible.

PBS was selected as the solvent for incubating the probe with cells. Initially, HepG2 cells were treated with **PTC** for 30 min, followed by the addition of F^- for another 30 min, and the fluorescence changes were observed. The probe itself exhibited weak fluorescence in the green channel, but upon the addition of F^-, fluorescence intensity notably increased in this channel (Fig. 7), indicating the applicability of probe **PTC** for fluorescent imaging of F^- within living cells.

Conclusion

In summary, utilizing thiophene boronic acid ester as a starting material, the probe **PTC** was designed and synthesized, which exhibits specific recognition towards F^-. This probe demonstrates good photophysical properties in DMSO solution, showing a good linear fluorescence response in the F^- concentration range of 0 to 12.5 μM ($R^2 = 0.98773$). It possesses a low detection limit (0.51 μM), rapid response

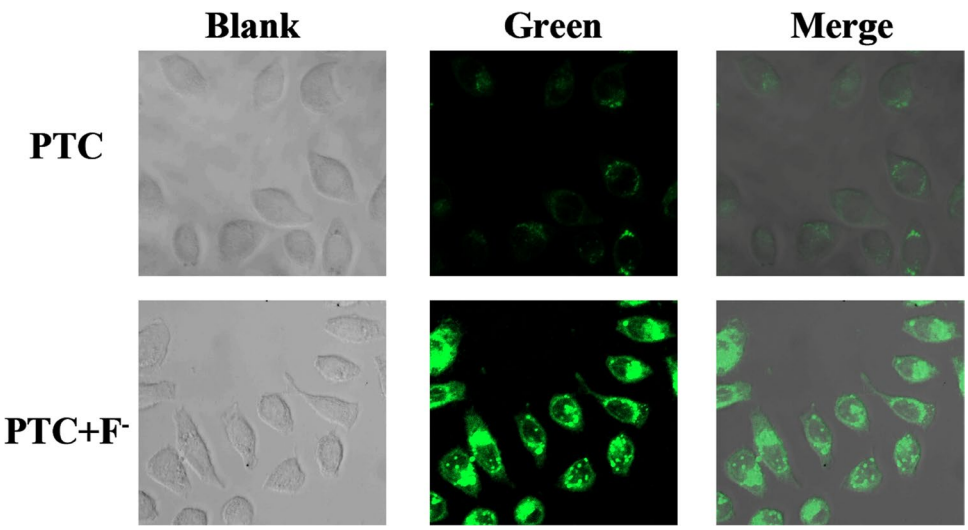

Fig. 7 Cell imaging of HepG2 cells co-incubated with **PTC** (3 μM in PBS) and F^- (100 μM), $\lambda_{ex} = 488$ nm

rate (reaching peak within 5 min), and significant color change of the solution before and after response (colorless to pink), which is discernible to the naked eye. Furthermore, it exhibits strong interference resistance, low cytotoxicity, and is suitable for live cell imaging, holding promise for further development as a rapid detection reagent for F^- in biological systems.

Supplementary Information The online version contains supplementary material available at https://doi.org/10.1007/s10895-024-03856-w.

Acknowledgements The authors are grateful for the financial support from the Guizhou University SRT Program (2023SRT587).

Author Contributions *Ying Zhang*: synthesis, test of probe properties and writing–original draft. *Tingting Feng*: NMR spectroscopy analysis and cell bioimaging. *Taozhu Hu* and *Yi Wang*: material preparation and instrument maintenance. *Yi Le*: software, validation, resources, writing–review & editing, supervision. All authors contributed to the study conception and design. All authors read and approved the final manuscript.

Funding Guizhou University SRT Program (2023SRT587).

Data Availability The date that support the findings of this study are available from the corresponding author upon reasonable request.

Declarations

Ethical Approval Not available.

Competing Interests The authors have no competing interests with the work presented in this manuscript.

References

1. Han J, Kiss L, Mei H, Remete AM, Ponikvar-Svet M, Sedgwick DM, Roman R, Fustero S, Moriwaki H, Soloshonok VA (2021) Chemical aspects of human and environmental overload with fluorine. Chem Rev 121:4678–4742. https://doi.org/10.1021/acs.chemrev.0c01263
2. Karunanidhi D, Aravinthasamy P, Subramani T, Roy PD, Srinivasamoorthy K (2020) Risk of fluoride-rich groundwater on human health: remediation through managed aquifer recharge in a hard rock terrain, South India. Nat Resour Res 29:2369–2395. https://doi.org/10.1007/s11053-019-09592-4
3. Singh J, Singh P, Singh A (2016) Fluoride ions vs removal technologies: A study. Arab J Chem 9:815–824. https://doi.org/10.1016/j.arabjc.2014.06.005
4. Torra M, Rodamilans M, Corbella J (1998) Serum and urine fluoride concentration: Relationships to age, sex and renal function in a non-fluoridated population. Sci Total Environ 220:81–85. https://doi.org/10.1016/S0048-9697(98)00248-4
5. Moreno EC, Kresak M, Zahradnik RT (2009) Physicochemical aspects of fluoride-apatite systems relevant to the study of dental caries. Caries Res 11:142–171. https://doi.org/10.1159/000260299
6. Zhu ZL, Yu HY, Zeng Q, He HW (2008) Characterization and biocompatibility of fluoridated biphasic calcium phosphate ceramics. Appl Surf Sci 255:552–554. https://doi.org/10.1016/j.apsusc.2008.06.055
7. Eggert F, Neubert R (1999) In vitro investigation of the liberation of fluoride ions from toothpaste compounds in a permeation model. Eur J Pharm Biopharm 47:169–173. https://doi.org/10.1016/S0939-6411(98)00060-5
8. Winter GB (1983) Fluorides in the prevention of caries. Arch Dis Child 58:485–487. https://doi.org/10.1136/adc.58.7.485
9. Usuda K, Kono K, Dote T, Nishiura K, Miyata K, Nishiura H, Shimahara M, Sugimoto K (1997) Urinary biomarkers monitoring for experimental fluoride nephrotoxicity. Arch Toxicol 72:104–109. https://doi.org/10.1007/s002040050475
10. Wei Y, Zeng B, Zhang H, Chen C, Wu Y, Wang N, Wu Y, Shen L (2016) iTRAQ-based proteomics analysis of serum proteins in wistar rats treated with sodium fluoride: insight into the potential mechanism and candidate biomarkers of fluorosis. Int J Mol Sci 17:1644
11. Ayoob S, Gupta AK (2006) Fluoride in drinking water: a review on the status and stress effects. Crit Rev Environ Sci Technol 36:433–487. https://doi.org/10.1080/10643380600678112
12. Xie K, Wang S, Yuan M, Zhang H, Deng H, Zhang Y, Wang J, Zhuang Y (2022) Tailored defect-rich cerium metal organic frameworks for efficient fluoride removal from wastewater. Sep Purif Technol 302:122152. https://doi.org/10.1016/j.seppur.2022.122152
13. Marquis RE, Clock SA, Mota-Meira M (2003) Fluoride and organic weak acids as modulators of microbial physiology. FEMS Microbiol Rev 26:493–510. https://doi.org/10.1111/j.1574-6976.2003.tb00627.x
14. Spira L (1962) Fluorine-induced endocrine disturbances in mental illness. Psychiatry Clin Neurosci 16:4–14. https://doi.org/10.1111/j.1440-1819.1962.tb01929.x
15. Liu Y, Jiang A, Jia Q, Zhai X, Liu L, Ma L, Zhou J (2018) Rationally designed upconversion nanoprobe for simultaneous highly sensitive ratiometric detection of fluoride ions and fluorosis theranostics. Chem Sci 9:5242–5251. https://doi.org/10.1039/C8SC00670A
16. Cittanova M-L, Lelongt B, Verpont M-C, Geniteau-Legendre M, Wahbe F, Prie D, Coriat P, Ronco PM (1996) Fluoride ion toxicity in human kidney collecting duct cells. Anesthesiology 84:428–435. https://doi.org/10.1097/00000542-199602000-00022
17. Yan L, Li D, Le Y, Dong P, Liu L (2022) Phenothiazine-based fluorescent probe for fluoride ions and its applications in rapid detection of endemic disease. Dyes Pigm 201:110200. https://doi.org/10.1016/j.dyepig.2022.110200
18. Samanta T, Das N, Shunmugam R (2021) Intramolecular charge transfer-based rapid colorimetric in-field fluoride ion sensors. ACS Sustain Chem Eng 9:10176–10183. https://doi.org/10.1021/acssuschemeng.1c02344
19. Mu M, Ke X, Cheng W, Li J, Ji C, Yin M (2022) Perylenemonoimide-based colorimetric probe with high contrast for naked-eye detection of fluoride ions. Anal Chem 94:11470–11475. https://doi.org/10.1021/acs.analchem.2c00766
20. Li D, Tu S, Le Y, Zhou Y, Yang L, Ding Y, Huang L, Liu L (2023) Development of carbazole-based fluorescent probe for highly sensitive application in fluoride ion detection. Spectrochim Acta Part A Mol Biomol Spectrosc 285:121816. https://doi.org/10.1016/j.saa.2022.121816
21. Zhang Y, Qu Y, Zhang Y, Gao Y, Wang L (2022) Development of a fluorescent strategy for quantification of fluoride ions in foods and toothpaste. Chem Eng J 448:137631. https://doi.org/10.1016/j.cej.2022.137631
22. Ahmadijokani F, Molavi H, Rezakazemi M, Aminabhavi TM, Arjmand M (2021) Simultaneous detection and removal of fluoride from water using smart metal-organic framework-based adsorbents. Coord Chem Rev 445:214037. https://doi.org/10.1016/j.ccr.2021.214037

23. Mandal TK, Hou Y, Gao Z, Ning H, Yang W, Gao M (2016) Graphene oxide-based sensor for ultrasensitive visual detection of fluoride. Advanced Science 3:1600217. https://doi.org/10.1002/advs.201600217
24. Wang Q, Li D, Rao N, Zhang Y, Le Y, Liu L, Huang L, Yan L (2021) Development of indole-based fluorescent probe for detection of fluoride and cell imaging of HepG2. Dyes Pigm 188:109166. https://doi.org/10.1016/j.dyepig.2021.109166
25. Kovalchuk Y, Podurets A, Osmolovskaya O, Nugbienyo L, Bulatov A (2024) Layered double hydroxide nanoparticles for a smartphone digital image colorimetry-based determination of fluoride ions in water, milk and dental products. Food Chem 438:137999. https://doi.org/10.1016/j.foodchem.2023.137999
26. Zhu C-Q, Chen J-L, Zheng H, Wu Y-Q, Xu J-G (2005) A colorimetric method for fluoride determination in aqueous samples based on the hydroxyl deprotection reaction of a cyanine dye. Anal Chim Acta 539:311–316. https://doi.org/10.1016/j.aca.2005.03.002
27. Zhou H, Chua MH, Tan HR, Lin TT, Tang BZ, Xu J (2019) Ionofluorochromic nanoparticles derived from octapyrene-modified polyhedral oligomeric silsesquioxane organic frameworks for fluoride-ion detection. ACS Applied Nano Materials 2:470–478. https://doi.org/10.1021/acsanm.8b01958
28. Hu KK, Huang WX, Su YH, Hu RZ (2009) Simultaneous determination of fluorine and iodine in urine by ion chromatography with electrochemical pretreatment. Chin Chem Lett 20:1483–1486. https://doi.org/10.1016/j.cclet.2009.05.030
29. Zhang X, Li S, Ma H, Wang H, Zhang R, Zhang X-D (2022) Activatable NIR-II organic fluorescent probes for bioimaging. Theranostics 12:3345–3371. https://doi.org/10.7150/thno.71359
30. Tian M, Wu R, Xiang C, Niu G, Guan W (2024) Recent advances in fluorescent probes for cancer biomarker detection. Molecules 29:1168
31. Tu S, Le Y, Yang L, Yi Q, Feng T, Yang J, Yang T, Wu T, Zhu W, Liu L (2024) Unraveling hydrogen sulfide detection and lysosome-mitochondria fusion in mitophagy using dual phenothiazine-based fluorescence probes. Sens Actuators, B Chem 406:135408. https://doi.org/10.1016/j.snb.2024.135408
32. Mengji R, Acharya C, Vangala V, Jana A (2019) A lysosome-specific near-infrared fluorescent probe for in vitro cancer cell detection and non-invasive in vivo imaging. Chem Commun 55:14182–14185. https://doi.org/10.1039/C9CC07322A
33. Luo Z, Huang Z, Li K, Sun Y, Lin J, Ye D, Chen H-Y (2018) Targeted delivery of a γ-glutamyl transpeptidase activatable near-infrared-fluorescent probe for selective cancer imaging. Anal Chem 90:2875–2883. https://doi.org/10.1021/acs.analchem.7b05022
34. Lin S, Ye C, Lin Z, Huang L, Li D (2024) Recent progress of near-infrared fluorescent probes in the determination of reactive oxygen species for disease diagnosis. Talanta 268:125264. https://doi.org/10.1016/j.talanta.2023.125264
35. Jiang G, Liu H, Liu H, Ke G, Ren T-B, Xiong B, Zhang X-B, Yuan L (2024) Chemical approaches to optimize the properties of organic fluorophores for imaging and sensing. Angew Chem Int Ed 63:e202315217. https://doi.org/10.1002/anie.202315217
36. He L, Xiong H, Wang B, Zhang Y, Wang J, Zhang H, Li H, Yang Z, Song X (2020) Rational design of a two-photon ratiometric fluorescent probe for hypochlorous acid with a large stokes shift. Anal Chem 92:11029–11034. https://doi.org/10.1021/acs.analchem.0c00030
37. Tian Y, Liu S, Cao W, Wu P, Chen Z, Xiong H (2022) H2O2-activated nir-II fluorescent probe with a large stokes shift for high-contrast imaging in drug-induced liver injury mice. Anal Chem 94:11321–11328. https://doi.org/10.1021/acs.analchem.2c02052
38. Tang B, Yu F, Li P, Tong L, Duan X, Xie T, Wang X (2009) A Near-infrared Neutral pH fluorescent probe for monitoring minor pH Changes: Imaging in living HepG2 and HL-7702 Cells. J Am Chem Soc 131:3016–3023. https://doi.org/10.1021/ja809149g
39. Wu L, Huang C, Emery BP, Sedgwick AC, Bull SD, He X-P, Tian H, Yoon J, Sessler JL, James TD (2020) Förster resonance energy transfer (FRET)-based small-molecule sensors and imaging agents. Chem Soc Rev 49:5110–5139. https://doi.org/10.1039/c9cs00318e